nature geoscience

SUPPLEMENTARY INFORMATION

https://doi.org/10.1038/s41561-019-0329-3

In the format provided by the authors and unedited.

Interruption of two decades of Jakobshavn Isbrae acceleration and thinning as regional ocean cools

Ala Khazendar[1]*, Ian G. Fenty[1], Dustin Carroll[1], Alex Gardner[1], Craig M. Lee[2], Ichiro Fukumori[1], Ou Wang[1], Hong Zhang[1], Hélène Seroussi[1], Delwyn Moller[3], Brice P. Y. Noël[4], Michiel R. van den Broeke[4], Steven Dinardo[1] and Josh Willis[1]

[1]Jet Propulsion Laboratory, California Institute of Technology, Pasadena, CA, USA. [2]Applied Physics Laboratory, University of Washington, Seattle, WA, USA. [3]Remote Sensing Solutions, Barnstable, MA, USA. [4]Institute for Marine and Atmospheric Research Utrecht, Utrecht University, Utrecht, The Netherlands. *e-mail: ala.khazendar@jpl.nasa.gov

Interruption of two decades of Jakobshavn Isbrae acceleration and thinning as regional ocean cools

Sensitivity of glacier change to other external forcings

We discuss here in more details other processes that could influence the behavior of Jakobshavn Isbrae.

An external mechanism hypothesized to perturb the stress regime at the front of the glacier is ice mélange variability. Ice mélange, a floating aggregate of icebergs and sea ice in the fjord, has been shown to modulate calving on seasonal timescales hence affecting glacier flow[1,2,3,4]. Whether that effect is relevant on interannual and decadal timescales remains an open question. In addition, it has been suggested that the general reduction of sea ice duration and thickness in recent years might be diminishing the ability of ice mélange to have an impact on calving[2]. In the case of Jakobshavn, the synchronous slowing and thickening of the three glaciers around Ilulissat Icefjord makes it much more likely that they were responding to shared oceanic and atmospheric forcings, rather than to ice mélange conditions, at least in the latter years of the study period.

Cryo-hydrologic warming is another forcing mechanism that can modify the glacier's stress regime. Water from both surface melting and rain drains through crevasses and moulins and may warm and thereby weaken ice at depth resulting in faster glacier flow[5,6]. To assess the likely impact of this process, we construct a timeseries of summer (June, July and August) cumulative production of surface meltwater and rain in the lower reaches of Jakobshavn Isbrae (Methods). As expected, the temporal variability is similar to that of the subglacial discharge (Supplementary Fig. 16) as the water emerging at the grounding line originates from surface runoff. This makes it difficult to disentangle the effects of the variability of subglacial discharge and of cryo-hydrologic warming. Nonetheless, the effects of the two processes on glacier acceleration or slowdown are expected to reinforce each other. Despite this combined effect, the correlation between glacier thickness change and surface water production is not strong (correlation coefficient of -0.17, with a p-value of 0.59).

Supplementary figures

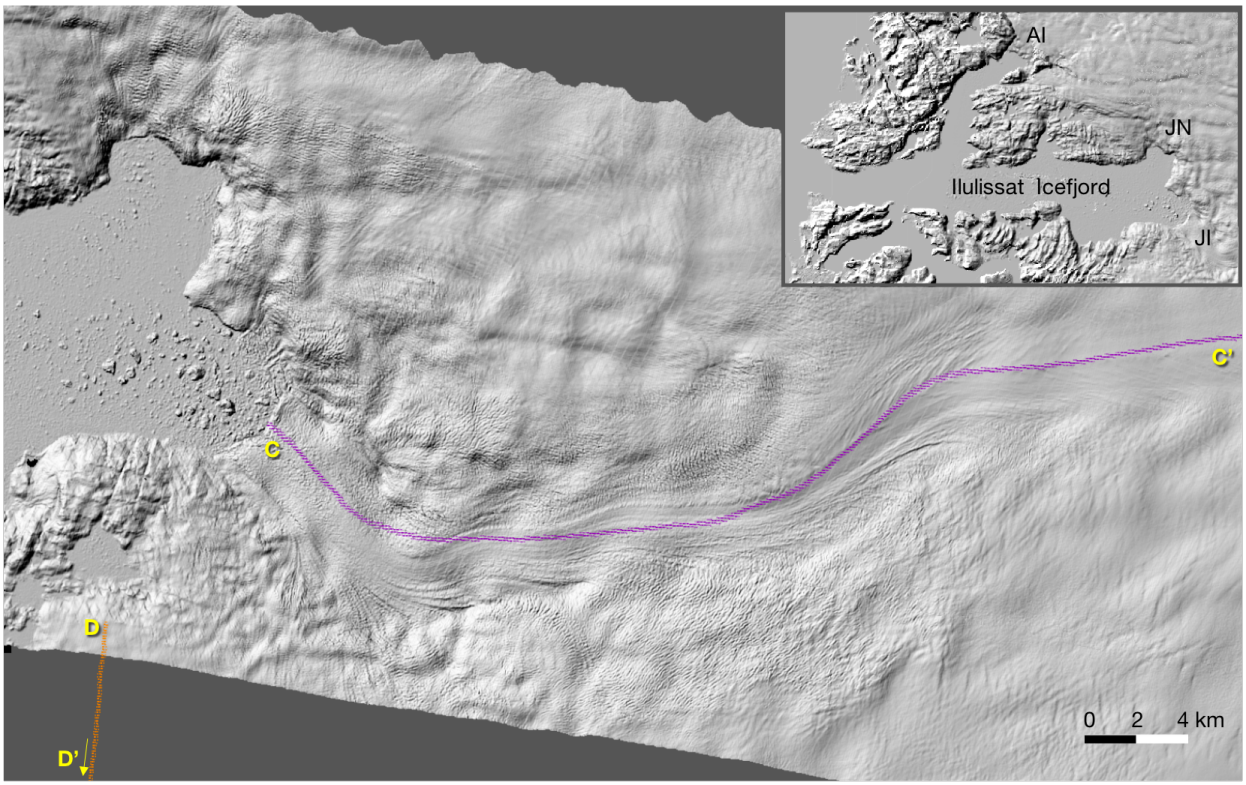

Supplementary Figure 1 | Jakobshavn Isbrae relief. The three overlapping swaths of the 2016 GLISTIN observation of Jakobshavn's main trunk shown in hill-shaded relief. The surface elevation changes shown in Supplementary Fig. 2 are found along the 2016 ATM ground track labeled CC'. Track DD', which extends beyond the frame of the figure over a total distance of 25 km, traverses a region of slow-moving ice (<200 m/yr) which we use to constrain the contribution of surface processes to the observed surface elevation change signal. **Inset** shows the locations of the three main glaciers terminating in Ilulissat Icefjord (AI: Avannarleq Ilulissat; JN: Jakobshavn Northern Branch; JI: Jakobshavn Isbrae). Image in inset combines the GLISTIN swaths and the 90-m Greenland Ice Mapping Project (GIMP) Digital Elevation Model[7].

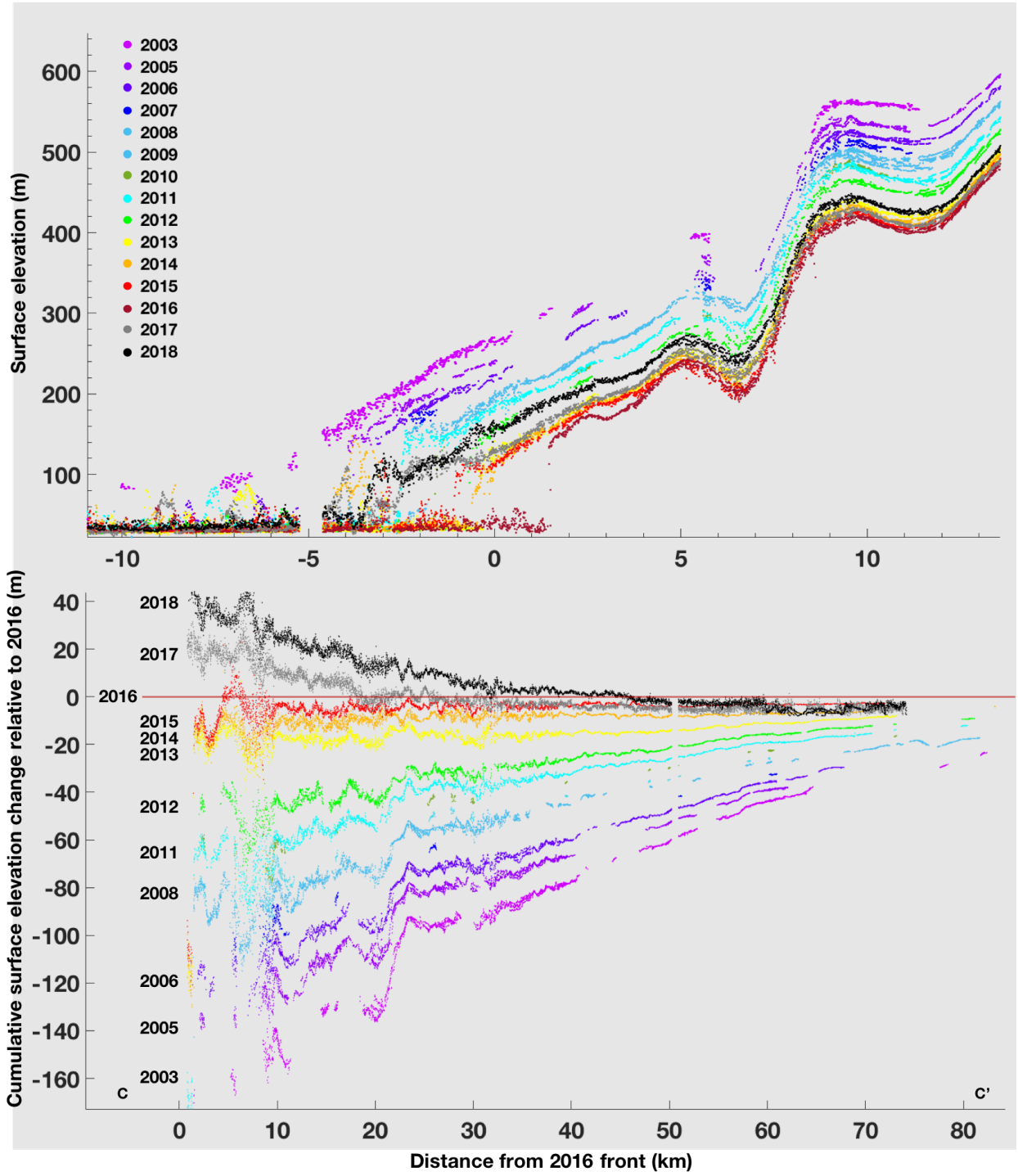

Supplementary Figure 2 | Jakobshavn Isbrae's surface elevation changes. Top panel shows elevations (relative to the WGS84 ellipsoid) of the lower reaches of the glacier during the period 2003-2018. The legend applies to both panels. **Bottom panel** depicts the cumulative changes in surface elevations. Change in elevation for each year is found relative to the year 2016, by subtracting the elevation of the earlier year from that of the latter. The path CC' (Supplementary Fig. 1) extends 80 km inland from the 2016 front. Data for the years 2003 to 2016 are from ATM observations, while the years 2017 and 2018 are from GLISTIN. During years missing from the time series the ATM track did not overlap with that of 2016. No smoothing is applied to the data. The uncertainty of the data is discussed in Methods.

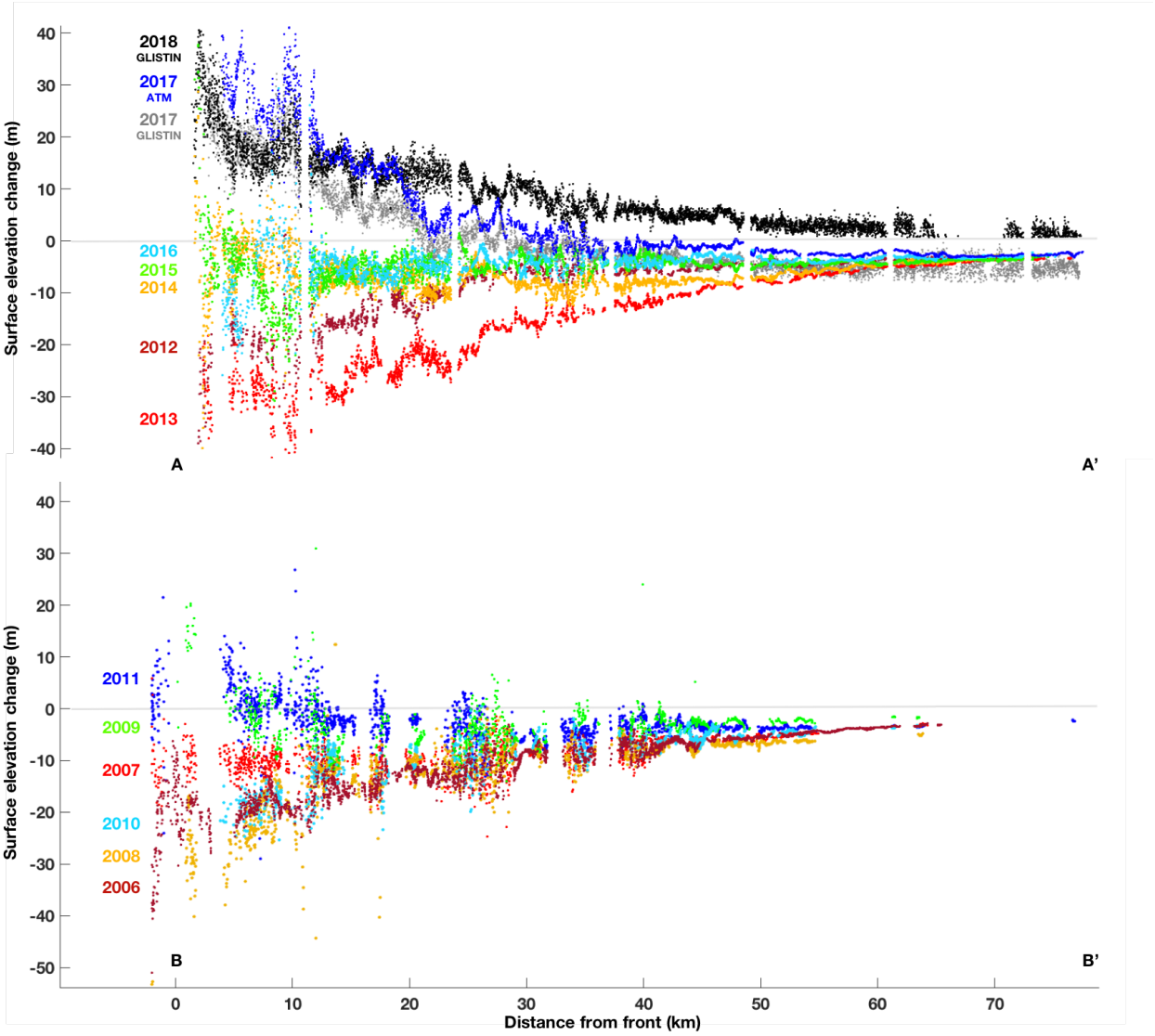

Supplementary Figure 3 | Surface elevation changes along the main trunk of Jakobshavn Isbrae. Changes in elevation for each year shown are found relative to the preceding year. The distance along path AA' is relative to the point where the 2017 ATM track intersects the 2017 front (Fig. 1; dates are given in Supplementary Table 1). Similarly, the distance along path BB' is relative to the point where the 2011 ATM track intersects the 2011 front (Fig. 1; dates are given in Supplementary Table 1). We interpolated the GLISTIN observations of elevation change (Fig. 1) along the 2017 ATM path, as shown in the top panel. The top panel is the same as in Fig. 2, except that no smoothing is applied here, and that we show the 2017 ATM data. The 2018 ATM data were not available at the time of writing. The uncertainty of the data is discussed in Methods.

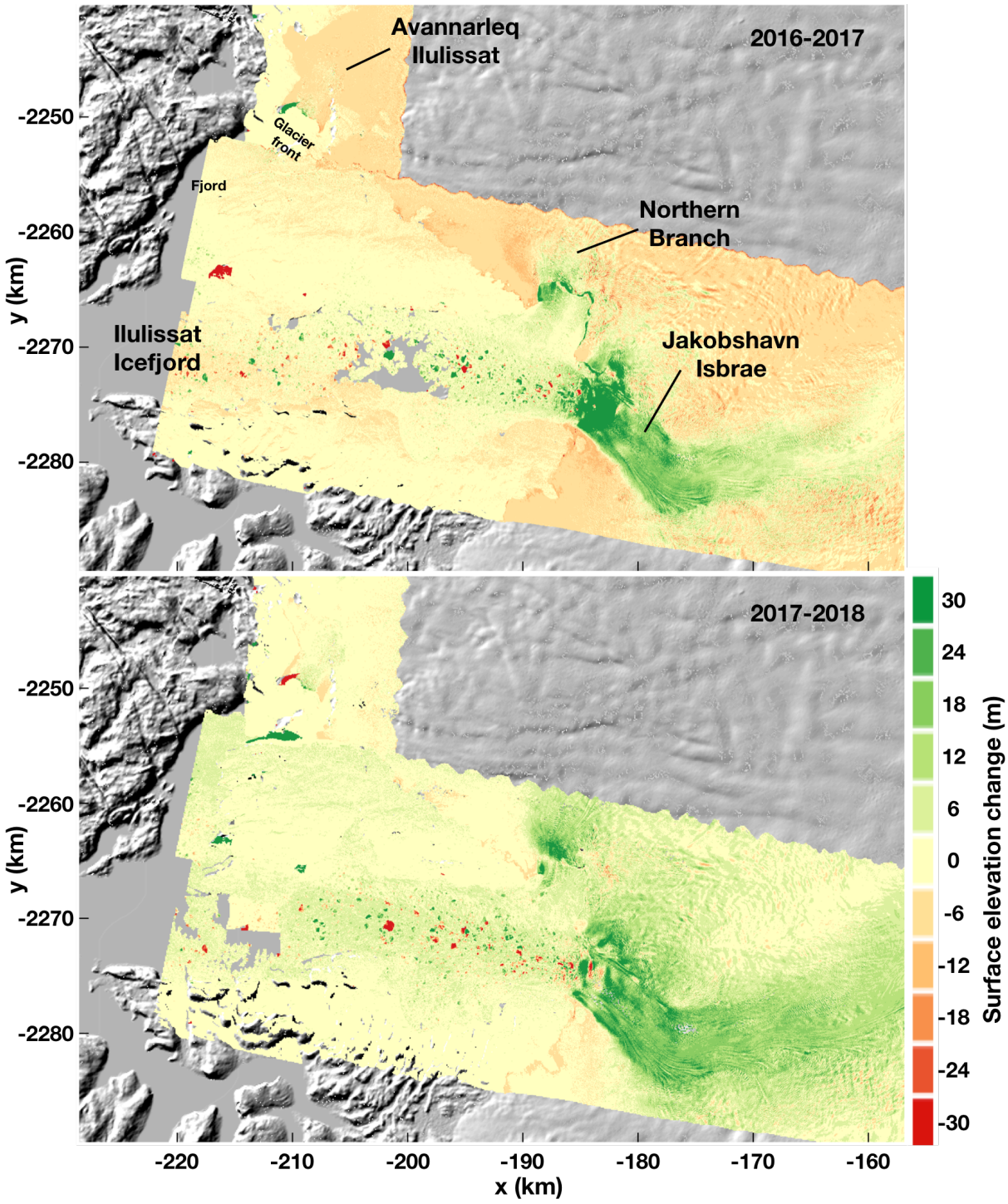

Supplementary Figure 4 | Surface elevation changes of Jakobshavn Isbrae, its Northern Branch and Avannarleq Ilulissat glacier. Changes in surface elevations for the periods 2016-2017 and 2017-2018 of the three main glaciers terminating in Ilulissat Icefjord. Measurements are by GLISTIN (Methods), and changes are obtained by subtracting the elevations of the earlier year from those of the latter. The color scale of elevation changes applies to both panels. The locations of the glaciers are shown in the inset of Supplementary Fig. 1.

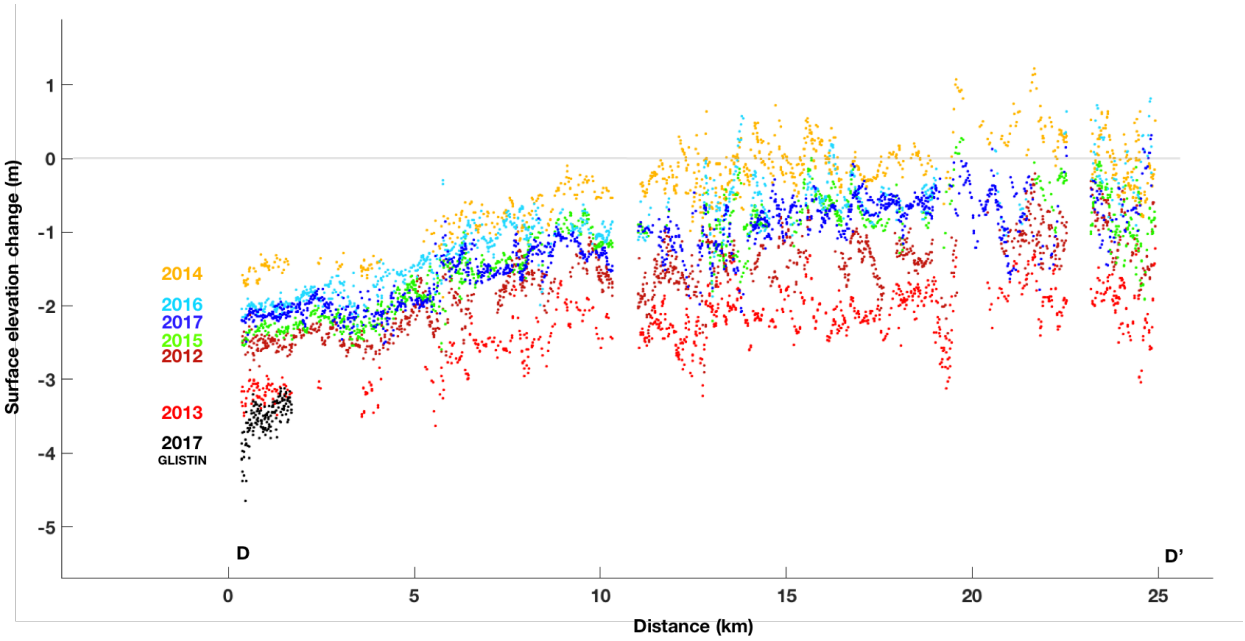

Supplementary Figure 5 | Surface elevation changes in a slow-moving ice area. Changes in elevation are along the path DD' (Supplementary Fig. 1), which traverses an area of slow-moving ice (slower than 200 m/yr). We use these measurements to constrain the contribution of surface processes such as precipitation and melting to observed surface elevation changes. Changes in elevation for each year shown are found relative to the preceding year. The uncertainty of the data is discussed in Methods.

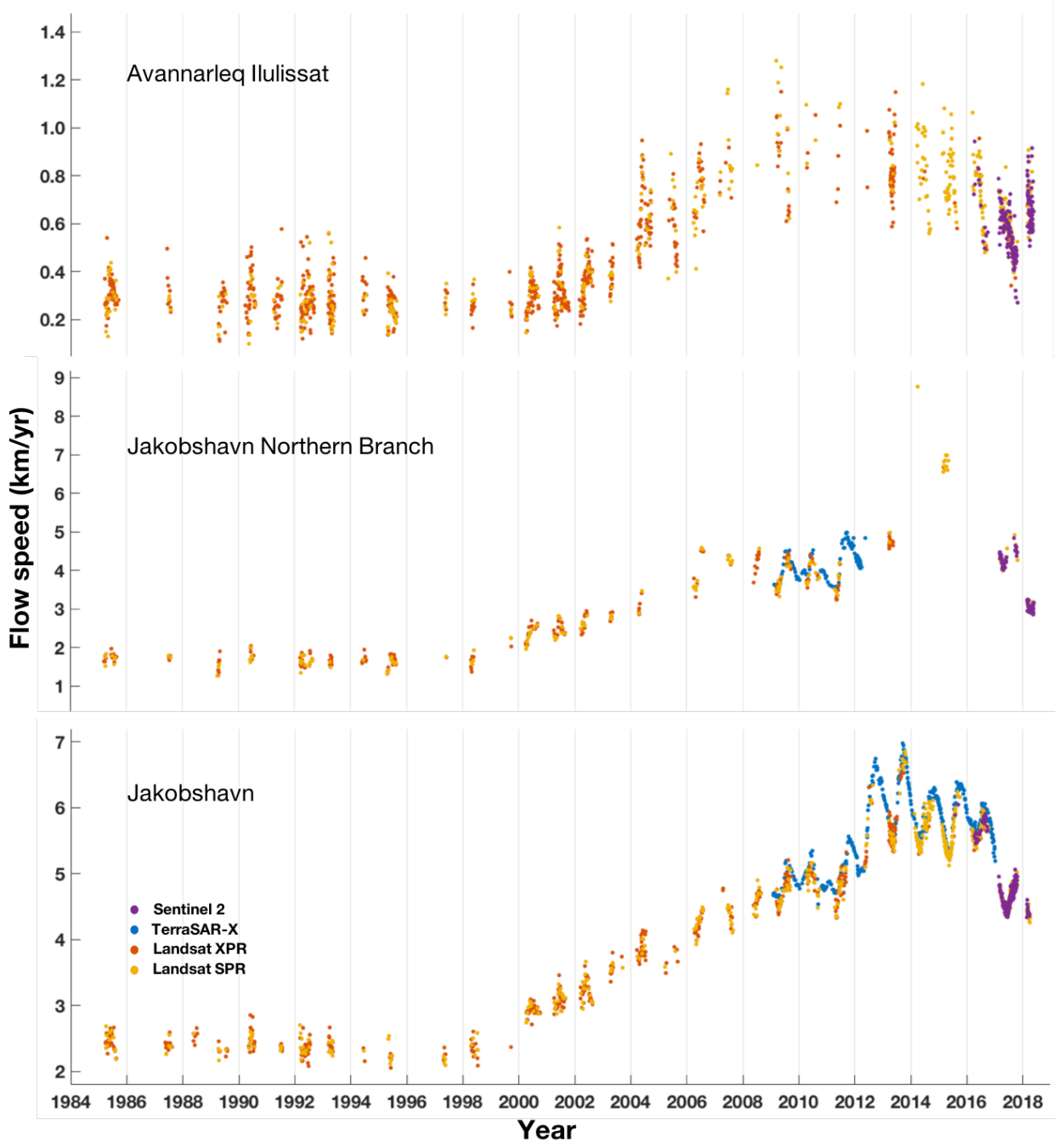

Supplementary Figure 6 | Flow speeds of the three main glaciers terminating in Ilulissat Icefjord. Glacier locations are shown in Supplementary Fig. 1. Time series extend from March 1985 to May 2018. Data are color coded by remote-sensing source and processing approach (XPR: Cross Path Row processing; SPR: Same Path Row processing).

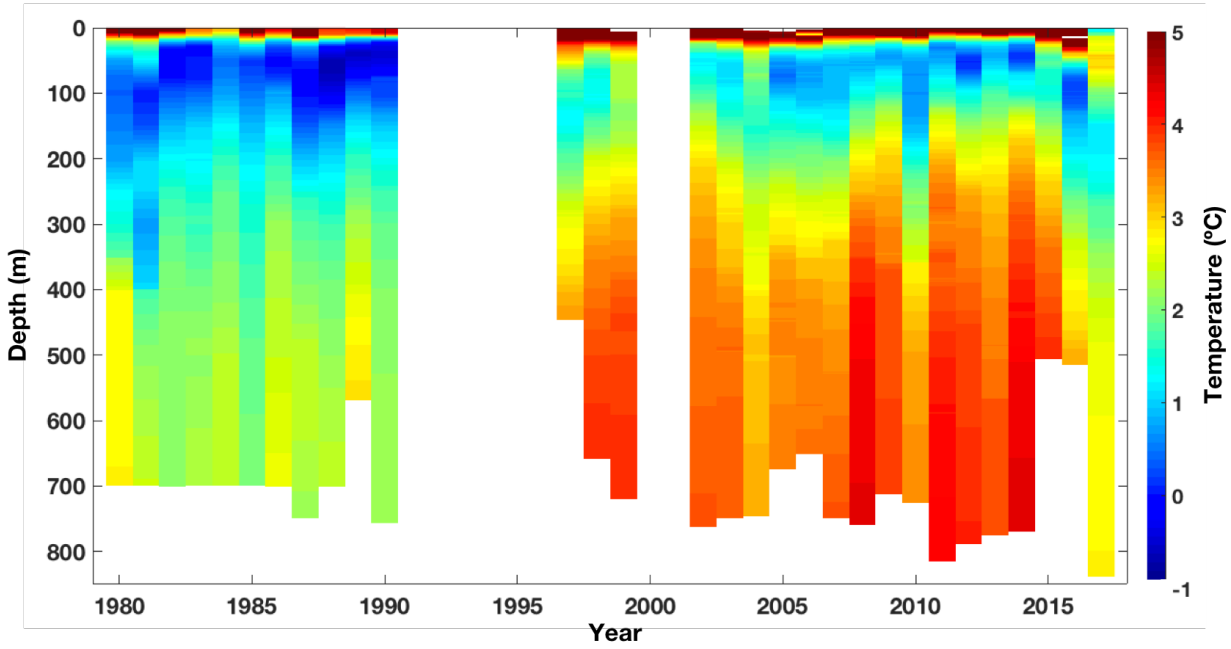

Supplementary Figure 7 | Temperatures in Disko Bay. Average temperatures in Disko Bay from CTD profiles collected in the locations indicated by the orange dots in Fig. 1b in the main text. Note the rapid cooling of the deep warm layer near the end of the time series.

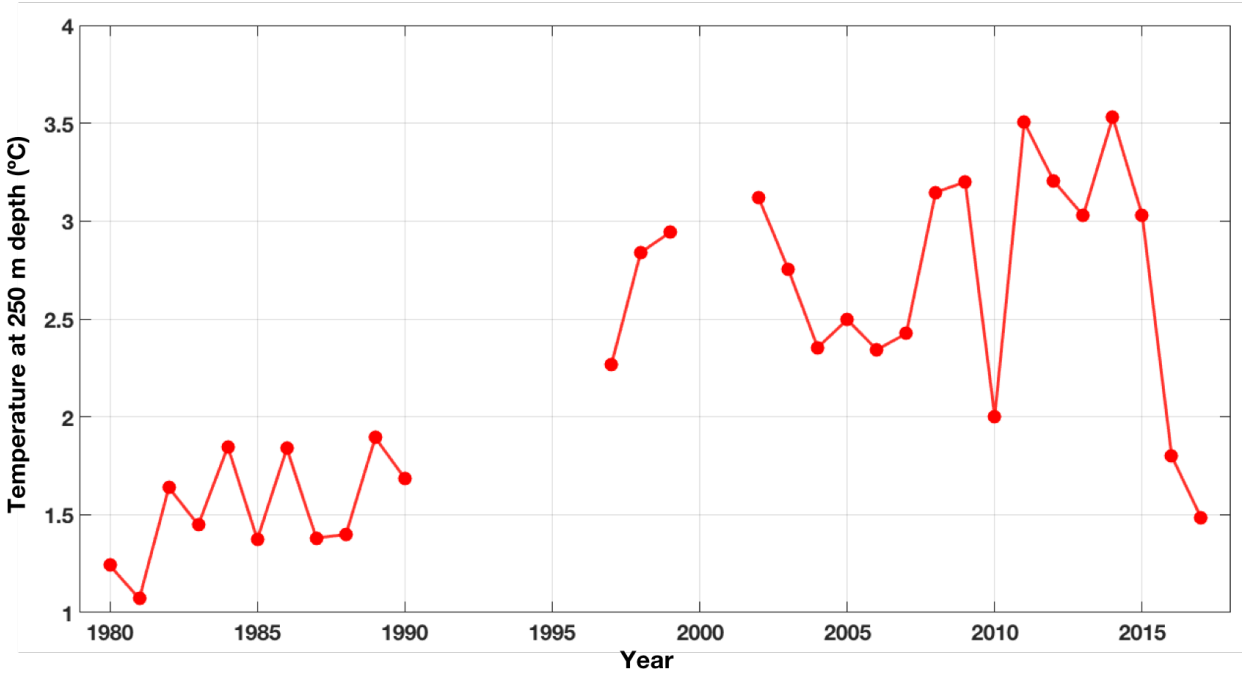

Supplementary Figure 8 | Temperatures in Disko Bay. As in Supplementary Fig. 7, but only for the depth at 250 m, which is the depth of the sill at the mouth of the fjord. Note that temperatures at 250-m depth have not been this cold since at least the early 1990s, and possibly since the late 1980s.

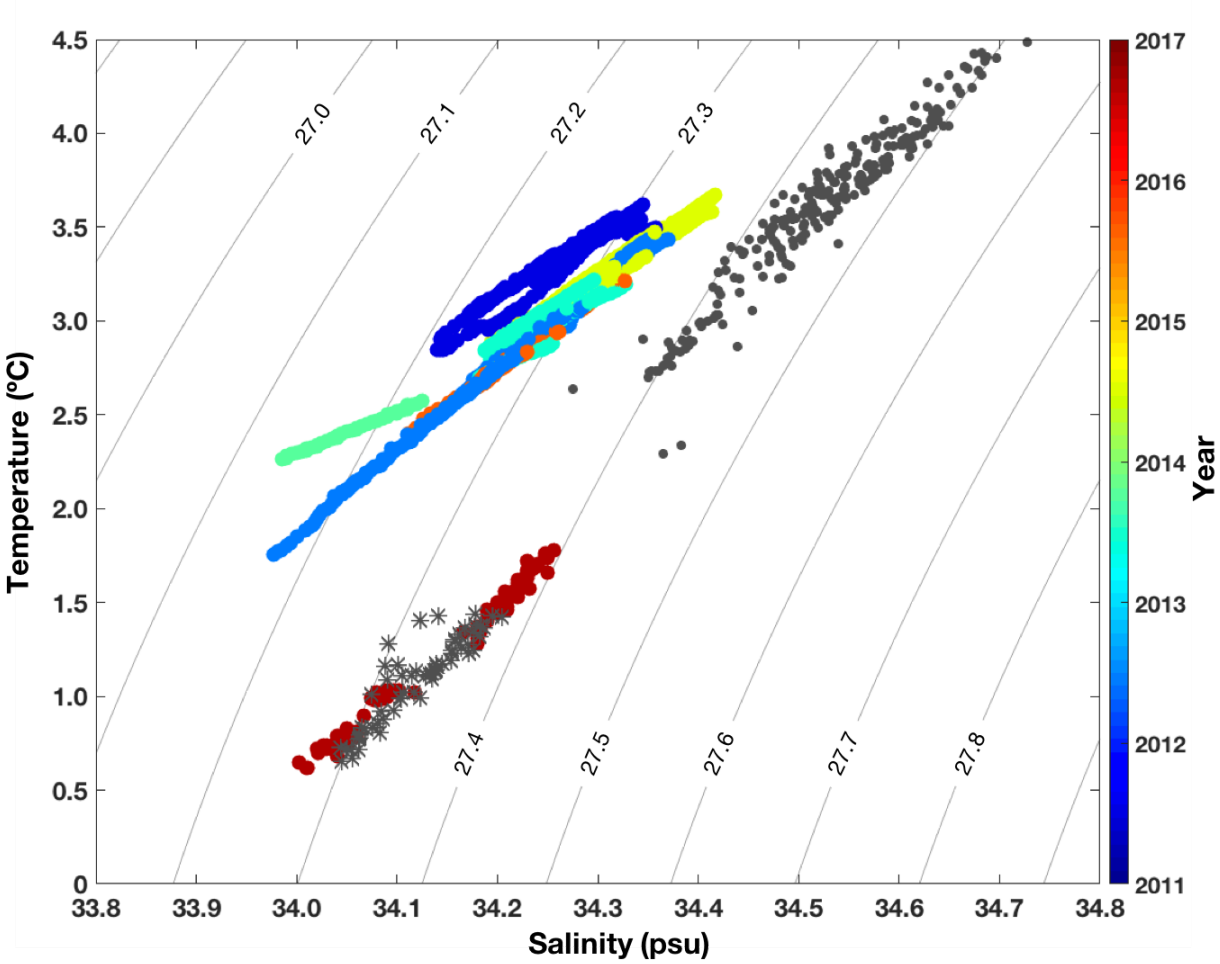

Supplementary Figure 9 | Temperature and Salinity in Disko Bay and Davis Strait. Temperature as a function of salinity for depths between 200 and 250 m in Disko Bay, compared with data from June and July at the moorings in Davis Strait. Contours show lines of constant potential density, minus 1000 kg/m^3. Colors show the various years of temperatures in Disko Bay. Dark grey dots show summer mooring data from Davis Strait for 2011 through 2015. Dark grey asterisks show mooring data in Davis Strait during summer of 2016. The large jump in properties in 2016 reflects a major change in temperature and salinity and the close correspondence with the properties of the mooring suggests that the cold water that arrived in Disko Bay in 2016 originated upstream. The June-July water in previous years is slightly heavier than the water in Disko Bay at these depths. This may be due in part to the fact that the mooring in 2016 was shallower (200 m, rather than 250 m), and slightly farther offshore, as well as some mixing with colder, fresher waters on the journey from Davis Strait to Disko Bay.

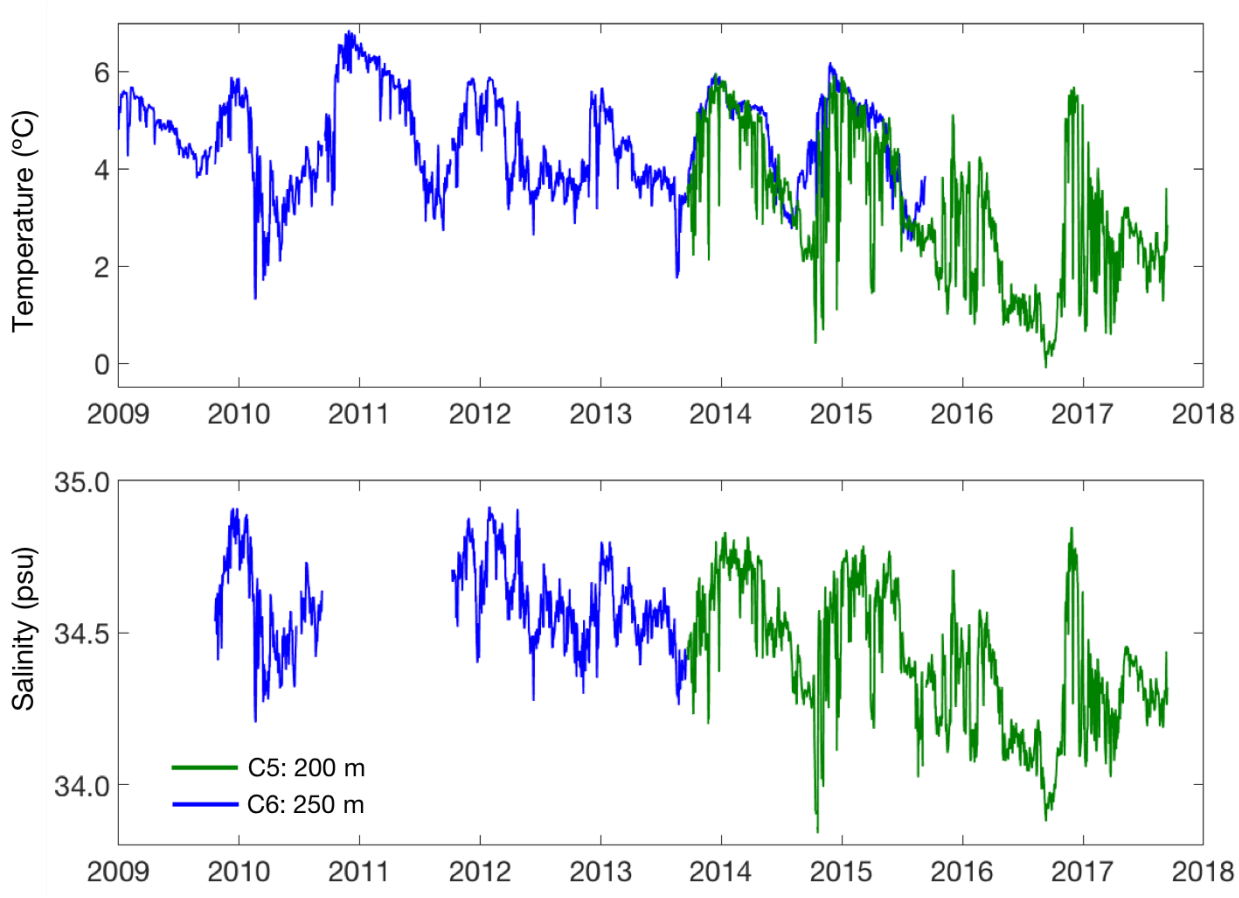

Supplementary Figure 10 | Temperature and Salinity in Davis Strait. Observations of daily-averaged temperature and salinity in Davis Strait at the location of two mooring (C5 and C6, shown as red dots in Fig. 3a of the main text). Although the C5 record is at 200 m depth and that of C6 is at 250 m depth, their variability is closely related and they are at the relevant depths to sample water at the correct density to make it over the sill and into Ilulissat Fjord (see ref. [8], Figure 2).

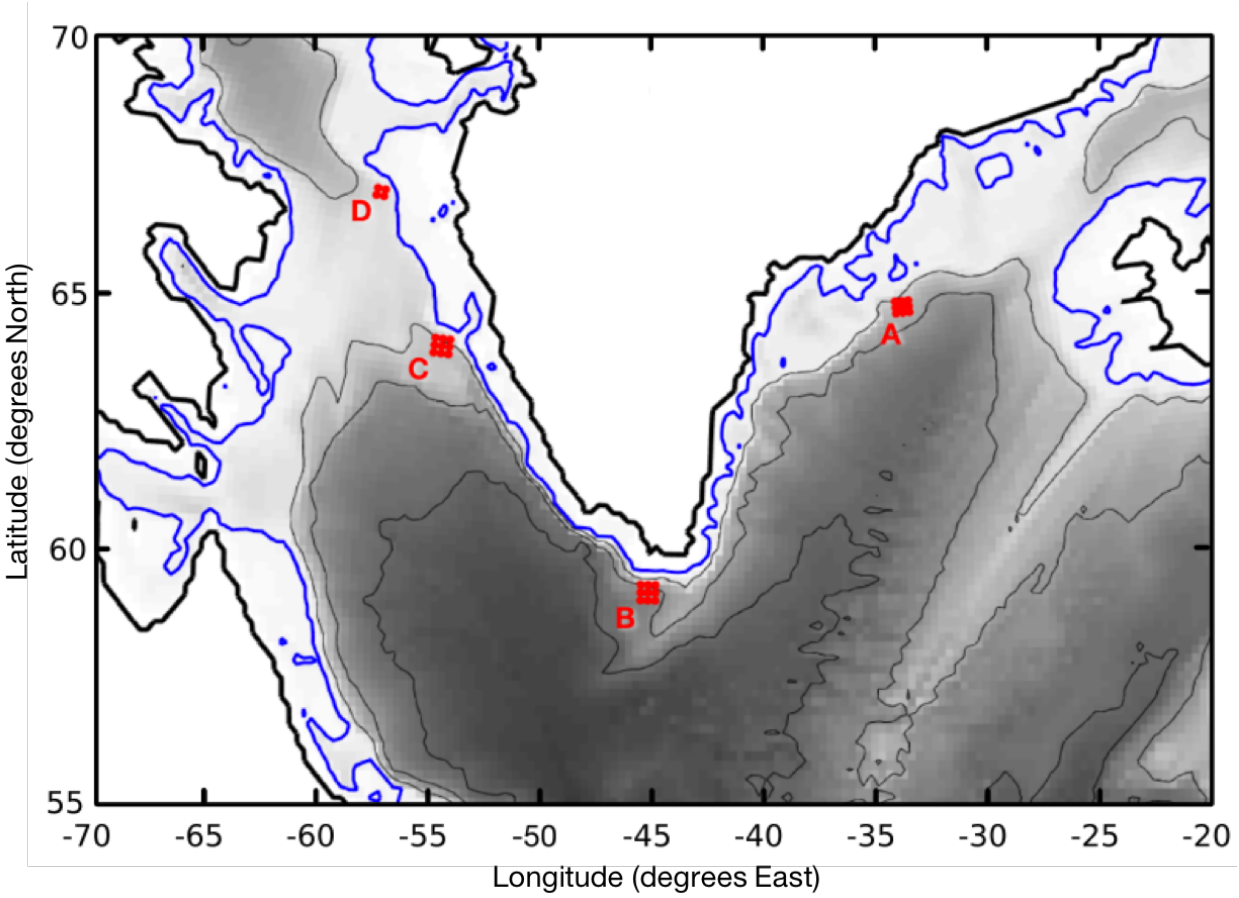

Supplementary Figure 11 | Locations of ocean temperature analysis. Atlantic Water enters the East Greenland boundary current near **A**. Cape Desolation at the southern tip of Greenland is marked by **B.** Point **C** is at the bifurcation of the 1000-m isobath from the Greenland continental slope towards Baffin Island, the southern end of the saddle separating the Labrador Sea from Baffin Bay. The Davis Strait moorings analyzed in this work are situated at **D.** In a typical year, the ECCO state estimate shows seasonal temperature maxima at 250 m depth in Nov at point **A**, Dec at **B**, Jan at **C**, Feb-Mar at **D.** Blue lines indicate the 250-meter isobath. Black contours are isobaths every 1000 m. The red dots are the model grid cells over which results were averaged to produce the time series in Supplementary Figs. 12,14 and15.

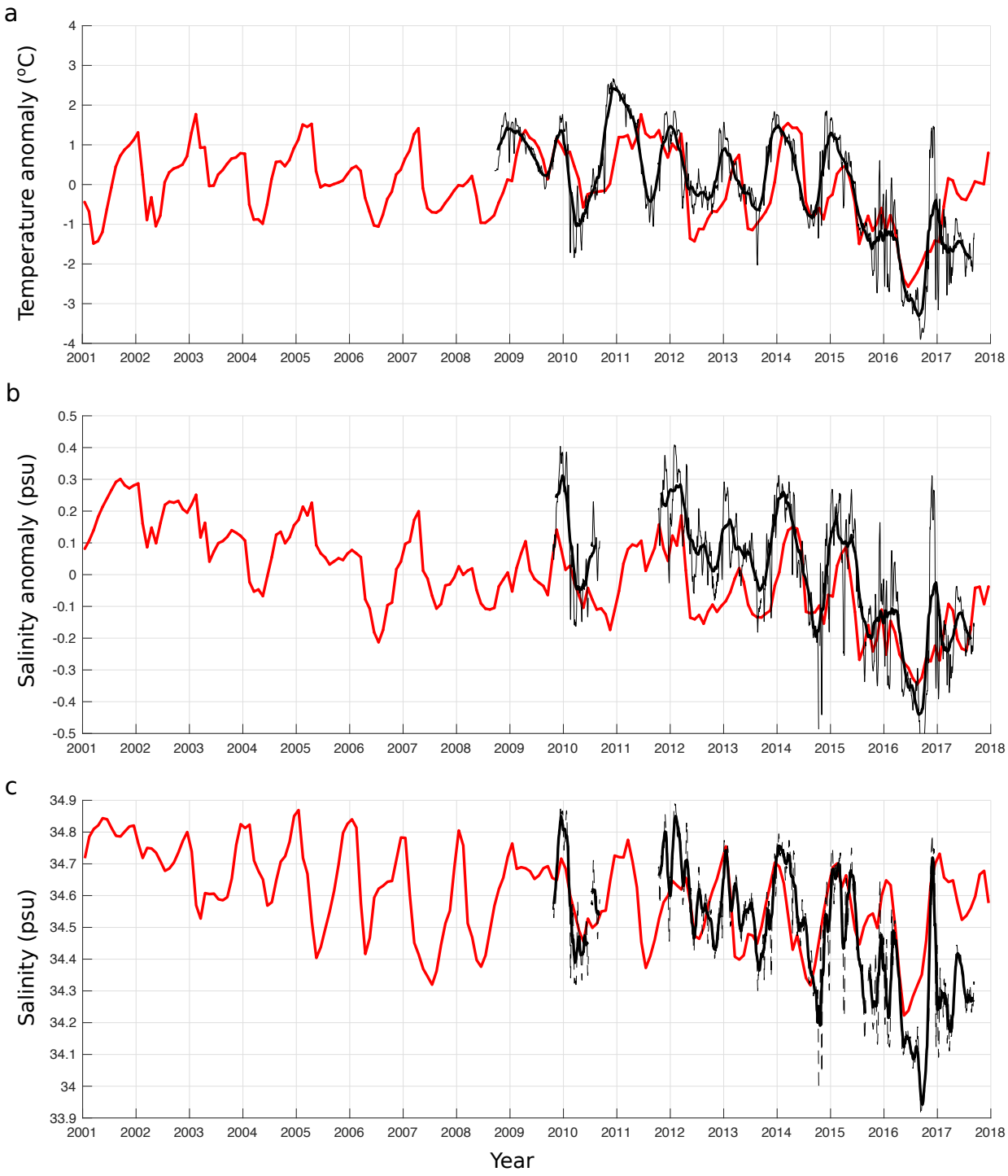

Supplementary Figure 12 | Temperature and salinity anomalies relative to 2009-2017 mean and the salinity at site of Davis Strait moorings. a, and b, Site is at point D in Supplementary Fig. 11. Red: ECCO state estimate; black: mooring data (heavy) 31-day boxcar averaged, (thin) 7-day boxcar averaged. We show the anomalies here because the ECCO state

estimate has a cold bias of 1°C relative to the mooring at this depth that is likely due to the model's resolution at this location (~11 km). The ECCO state estimate captures the timing and magnitude of seasonal and interannual variations very well and therefore can be analyzed to determine their origin. **c,** Salinity from the mooring at Davis Strait (point D) and from upstream in the ECCO state estimate (point C). Red: ECCO state estimate, black: mooring data (heavy) 31-day boxcar averaged, (thin) 7-day boxcar averaged. These salinity time series compliment Fig. 3e in the main text that shows the equivalent for temperature. The ECCO state estimate upstream reproduces the timing and magnitudes of the seasonal and interannual variations seen at the downstream mooring which suggests that the variations seen at the mooring originate upstream.

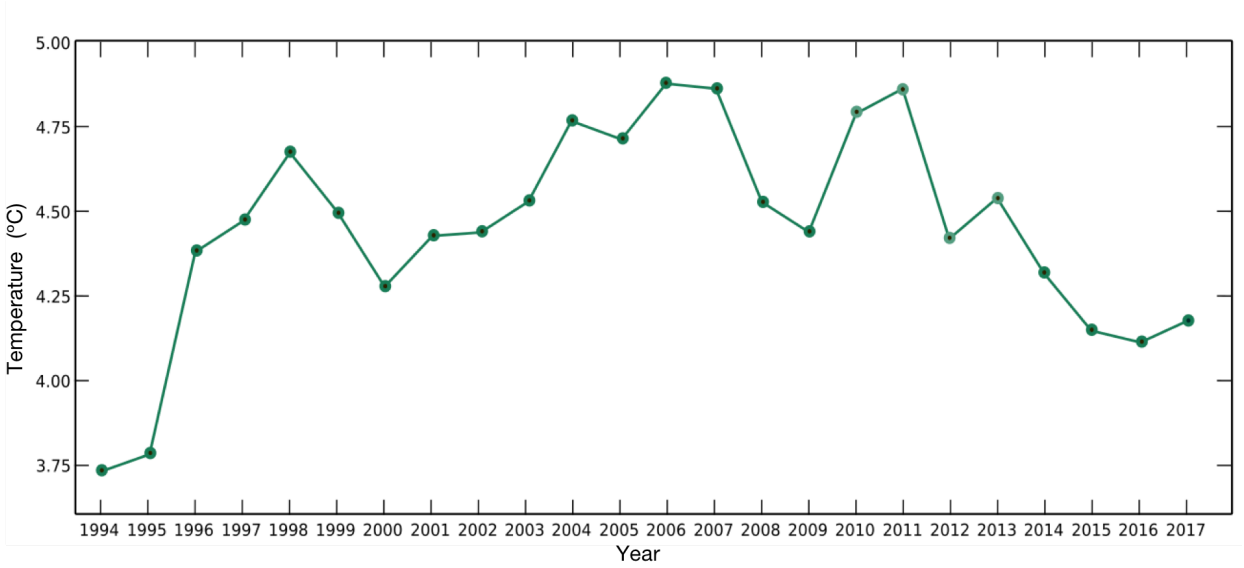

Supplementary Figure 13 | Subpolar Gyre temperatures. Depth-averaged (0-300 m) upper ocean temperatures estimated from the ECCO model and Argo observations for the period 2015 to 2017 (ref. [9]) within the Subpolar Gyre.

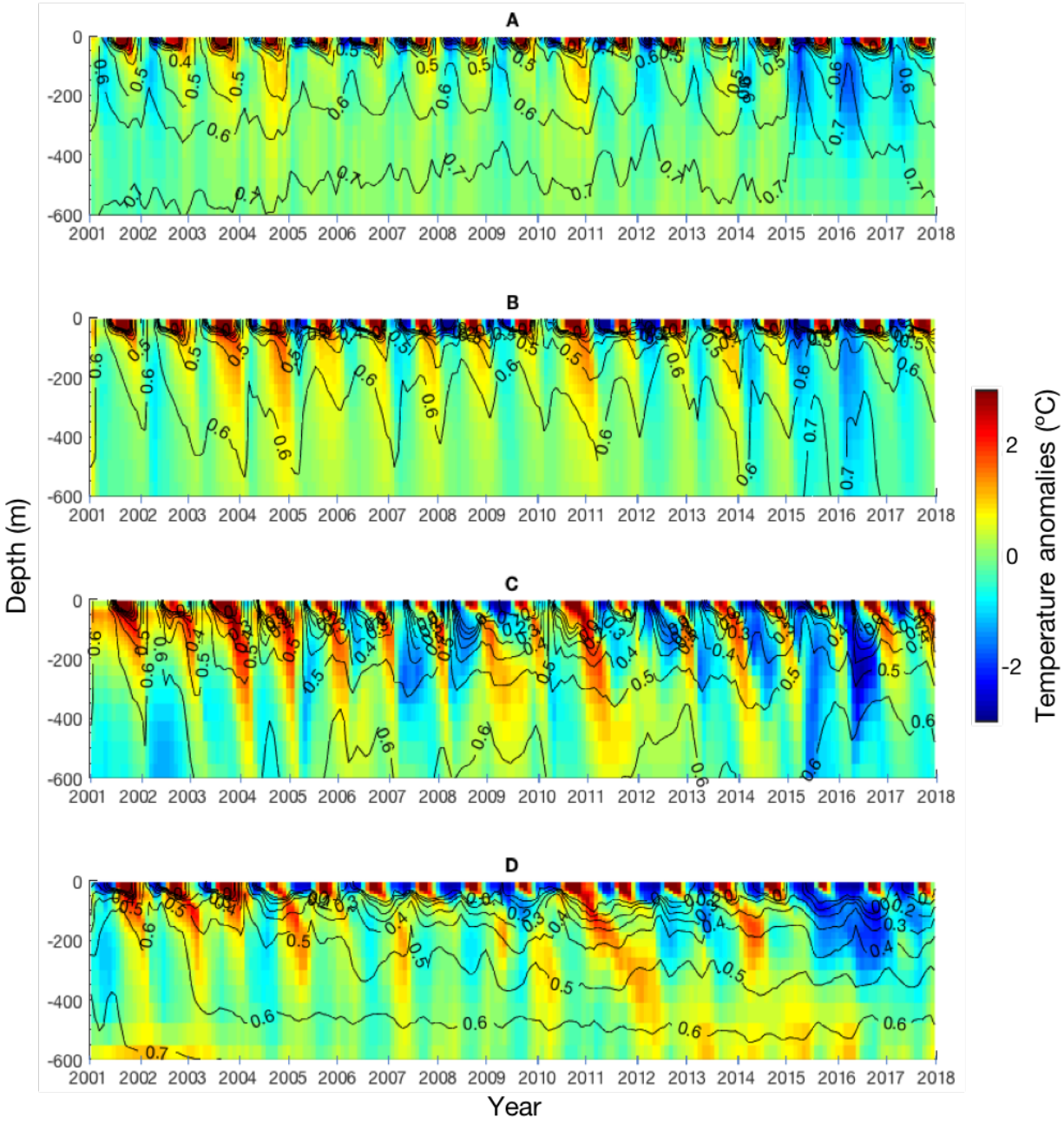

Supplementary Figure 14 | Depth-time evolution of temperature anomalies at the four sites A-D (shown in Supplementary Fig. 11) from the ECCO state estimate. Anomalies at each depth are relative to the mean over the period 2001 to 2017. Surface-referenced potential density contours, ρ_0 -1027 kg/m^3, are overlaid. Large wintertime (DJFM) air-sea heat fluxes in 2015 across the entire subpolar gyre induce cold anomalies at all points. Temperatures at **A** partially recover but remain 0.6° cooler than average. Points **B-D** are downstream of **A** and also show significantly reduced temperature recovery through 2015**.** Total 2016 Wintertime cooling at **C** and **D** drive temperatures to the coldest temperatures seen over the 2001-2018 period. Importantly, between **B-D** temperatures below 100 m do not recover as normal between spring and fall in 2016.

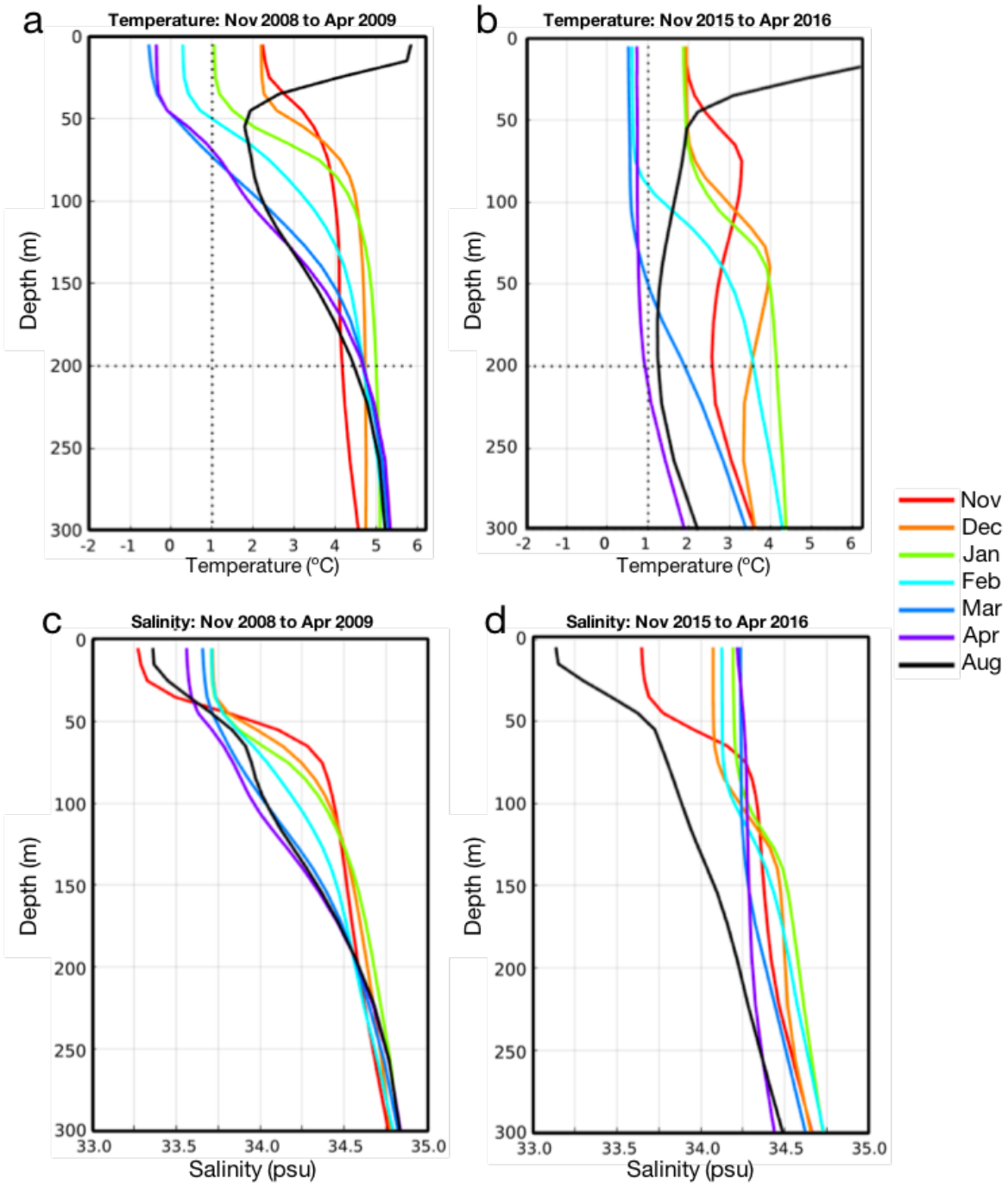

Supplementary Figure 15 | Evolution (Nov-Aug) of temperature (a-b) and salinity (c-d) at location C from the ECCO state estimate in two different years. The two years show distinct progression of mixed layer deepening and upper ocean cooling through winter (Nov-Mar). Winter 2009 (a, c) shows a mixed layer deepening to 50 m in Mar-Apr and cooling in upper 50 m by 2.5°C and little temperature change at 200 m (4.1°C in Nov). In contrast, the winter 2016 shows the evolution of a much deeper mixed layer (to ~220 m), and large cooling through the mixed layer of about 1.5°C. At 200-250 m, 2016 temperatures reach 1°C in Apr and remain close to 1°C in August. Relative to the 2001-2018 average, the 2015 initial upper ocean stratification (not shown) is weaker and temperatures in the upper 200 are colder.

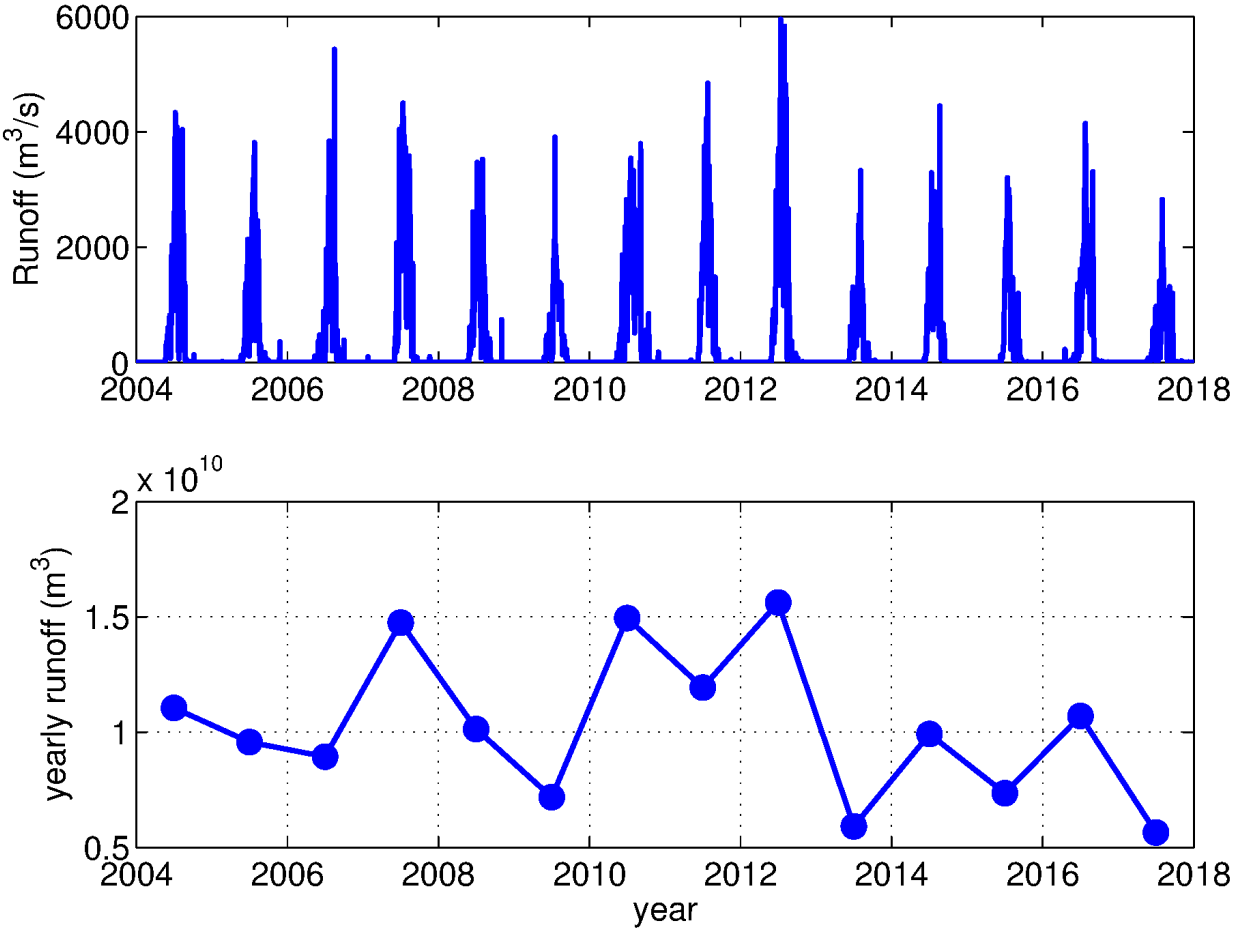

Supplementary Figure 16 | Subglacial discharge as estimated by RACMO2.3p2. Daily subglacial discharge (top panel) and the yearly-integrated values (bottom panel). Data are estimated using RACMO2.3p2 at 1 km resolution as discussed in the text. These were used as input for the plume model, in combination with temperature and salinity in Disko Bay as well as depth of the glacier at the calving front to compute the melting rate at the front.

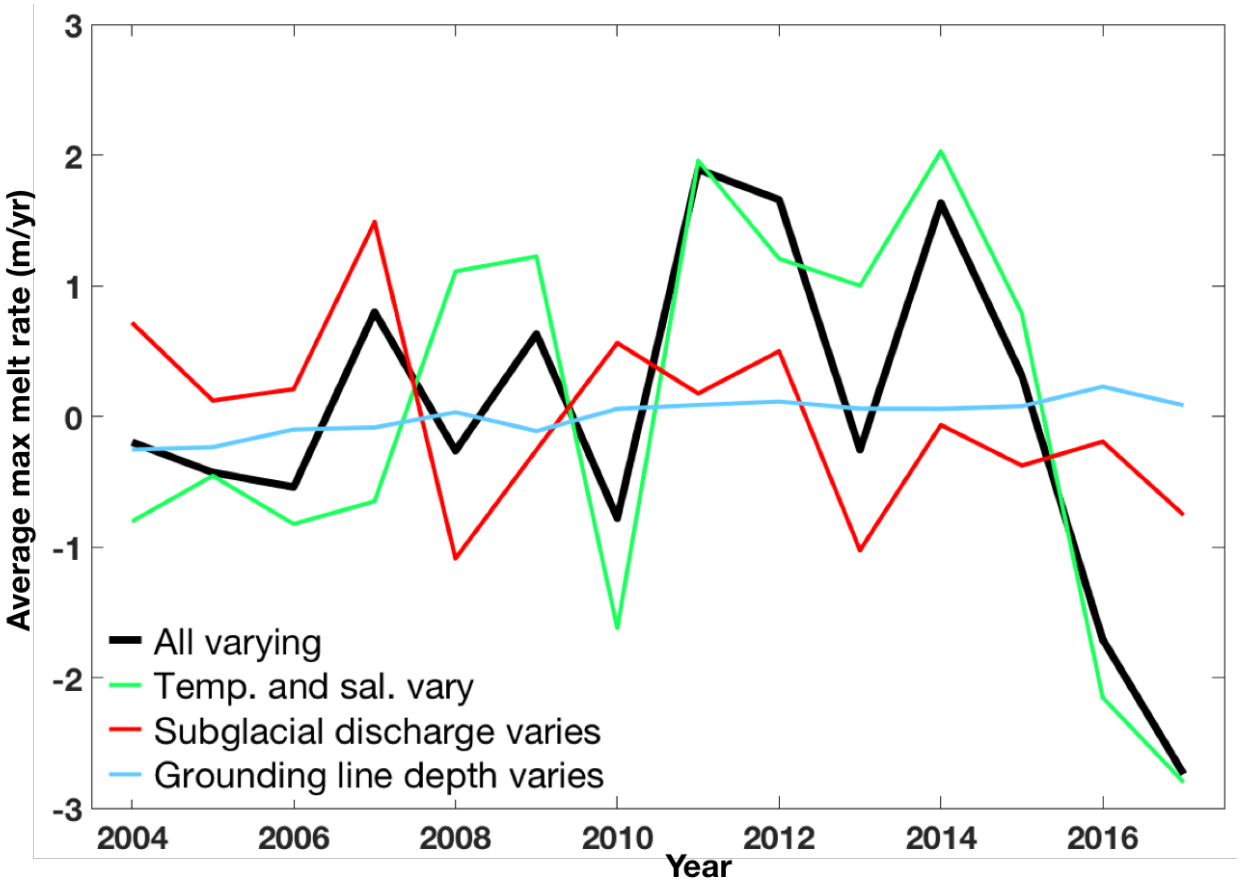

Supplementary Figure 17 | Sensitivity of plume model results to various inputs. Average of the maximum melt rate over a melt season for several different runs of the plume model. The time mean of each time series has been removed, since confidence in the model is highest for year-to-year variations. In the primary run, which was used for comparison with glacier response, temperature and salinity profiles at the glacier front, the depth below sea level of the glacier at the calving front or grounding line, and subglacial discharge were all allowed to vary from year to year. In the three other runs, two of these inputs where held constant at their mean values for each year and only one of these inputs was allowed to vary.

Supplementary tables

Supplementary Table 1 | Dates, front locations and averaged elevation changes. For each ATM data acquisition date, we attempted to find a useable Landsat image close in date to detect the front location. For the years 2005-2011, the front location for each was found relative to the 2011 front (used for the calculation in the last column), and relative to the 2017 front (used in the bed topography plot of Fig. 2 (inset)). Changes in surface elevation for each year are found relative to the preceding year, then the values for all points located 10 to 15 km upstream from the front are averaged. For each pair of years that enter into the calculation, the front location used to find the 10-15-km section is the front most upstream of the two years. We normalized the averaged surface elevation values by finding the rate of change per day for each pair of years then multiplying that by 365 days. If observations were made on several dates in a year, we used the earliest of those dates in calculating the number of days separating data acquisition among years.

Year	ATM acquisition dates	Front dates	Distance from 2011 front (km) | positive upstream	Distance from 2017 front (km) | positive upstream	Elevation changes averaged 10 to 15 km upstream from front (m)	Normalized elevation changes averaged 10 to 15 km upstream from front (m/yr)
2003	May 11	*Year not included in these analyses*				
2004	*No data*					
2005	May 14	June 16	-3.73	-3.18		
2006	May 26, 27, 28	May 27	-1.99	-1.51	-17.37	-16.82
2007	May 10	June 6	-2.08	-1.38	-10.67	-11.16
2008	July 10, 11, 17, 18, 22	July 17	0.89	0.68	-12.37	-10.57
2009	April 27, 28/May 5	May 1	-2.62	-1.75	-5.07	-6.36
2010	May 7, 14, 17	April27	1.44	1.14	-11.65	-11.34
2011	March 31/April 6, 7, 8, 16, 22, 26	April 7	0	-0.11	-2.00	-2.23
2012	April 11, 21, 29/May 2	May 18		2.44	-14.94	-14.46
2013	April 4, 6, 10	April 3		1.93	-25.91	-26.42
2014	April 9, 14, 19	April 14		1.87	-6.64	-6.55
2015	April 9, 11, 17, 21, 23, 25	April 24		1.48	-6.02	-6.02
2016	May 16	May 5		3.11	-5.62	-5.54
2017	April 29/May 1, 2, 6, 10	May 1		0	14.84	15.56

Supplementary Table 2 | Ice surface and bottom elevations, and hydrostatic equilibrium levels. A list of the data used in the calculation of the hydrostatic equilibrium level near the front location of each year. The calculation was made in each year ~1 km inland from the front for that year to increase the chances of avoiding undercut ice that might exist nearer to the front, and to avoid the most fractured ice that might affect the ATM surface detection. The distances between the 2011 reference front and the front location for each year are found along path BB' in Fig.1. The largest source of uncertainty in the calculation of hydrostatic equilibrium level is the uncertainty of bed depths, which in the study region varies between 15 and 100 m, as described in Methods. Bed depths are given relative to the geoid, and ATM surface elevations, which are relative to the WGS84 ellipsoid, are given here relative to the geoid by subtracting 27 m, which is local sea level as measured by ATM. Ice density used is 917 kg/m^3, and ocean water density is 1030 kg/m^3. The correlation between surface elevation changes shown in the last column of Supplementary Table 1 and heights above floatation shown in the last column of this and the following table is -0.36, with a p-value of 0.25.

Year	Distance From 2011 front (km)	Distance From 2011 Font where hydrostatic elevation is calculated (km)	ATM surface height (m)	Bed Depth (m)	Ice thickness (m)	Hydrostatic equilibrium level (m)	Difference (ATM height – hydrostatic level) (m)
2005	-3.73	-2.98	100	-687	787	86.34	13.66
2006	-1.99	-0.92	113.5	-775	888.5	97.48	16.02
2007	-2.08	-1.63	81	-744	825	90.51	-9.51
2008	0.89	1.23	134	-815	949	104.11	29.89
2009	-2.62	0.14	117.5	-834	951.5	104.39	13.11
2010	1.44	*No data near front*					

Supplementary Table 3 | Ice surface and bottom elevations, and hydrostatic equilibrium levels. As in Supplementary Table 2, but for the years 2011 to 2017. The distances between the 2017 reference front and the front location for each year are found along path AA' in Fig.1.

Year	Distance From 2017 front (km)	Distance From 2017 Front where hydrostatic elevation is calculated (km)	ATM surface height (m)	Bed Depth (m)	Ice thickness (m)	Hydrostatic equilibrium level (m)	Difference (ATM height – hydrostatic level) (m)
2011	-0.11	0.98	117.5	-828	945.5	103.73	13.77
2012	2.44	2.80	140.5	-879	1019.5	111.85	28.65
2013	1.93	3.23	119.0	-939	1058	116.07	2.93
2014	1.87	3.03	109.5	-917	1026.5	112.61	-3.11
2015	1.48	2.61	92.0	-867	959	105.21	-13.21
2016	3.11	5.09	144.4	-980	1124.4	123.36	21.04
2017	0	1.15	93.8	-835	928.8	101.9	-8.1

Supplementary references

1. Amundson, J. et al. Ice mélange dynamics and implications for terminus stability, Jakobshavn Isbræ, Greenland. *Journal of Geophysical Research* 115, (2010).
2. Cassotto, R., Fahnestock, M., Amundson, J., Truffer, M. & Joughin, I. Seasonal and interannual variations in ice mélange and its impact on terminus stability, Jakobshavn Isbræ, Greenland. *Journal of Glaciology* 61, 76-88 (2015).
3. Robel, A. Thinning sea ice weakens buttressing force of iceberg mélange and promotes calving. *Nature Communications* 8, 14596 (2017).
4. Joughin, I. et al. Continued evolution of Jakobshavn Isbrae following its rapid speedup. *Journal of Geophysical Research* 113, (2008).
5. Van Der Veen, C., Plummer, J. & Stearns, L. Controls on the recent speed-up of Jakobshavn Isbræ, West Greenland. *Journal of Glaciology* 57, 770-782 (2011).
6. Cavanagh, J., Lampkin, D. & Moon, T. Seasonal variability in regional ice flow due to meltwater injection into the shear margins of Jakobshavn Isbrae. *Journal of Geophysical Research: Earth Surface* 122, 2488-2505 (2017).
7. Howat, I., Negrete, A. & Smith, B. The Greenland Ice Mapping Project (GIMP) land classification and surface elevation data sets. *The Cryosphere* 8, 1509-1518 (2014).
8. Gladish, C. V., Holland, D. M. & Lee, C. M. Oceanic Boundary Conditions for Jakobshavn Glacier. Part II: Provenance and Sources of Variability of Disko Bay and Ilulissat Icefjord Waters, 1990–2011*. *Journal of Physical Oceanography* 45, 33–63 (2015).
9. Roemmich, D. & Gilson, J. The 2004–2008 mean and annual cycle of temperature, salinity, and steric height in the global ocean from the Argo Program. *Progress in Oceanography* 82, 81–100 (2009).